Case Studies in Thermal Engineering 28 (2021) 101518

Contents lists available at ScienceDirect

Case Studies in Thermal Engineering

journal homepage: www.elsevier.com/locate/csite

Effects of fractional derivative and heat source/sink on MHD free convection flow of nanofluids in a vertical cylinder: A generalized Fourier's law model

Nehad Ali Shah [a], Abderrahim Wakif [b], Rasool Shah [c], Se-Jin Yook [d,*], Bashir Salah [e], Yasir Mahsud [a], Kashif Hussain [a]

[a] Department of Mathematics, Lahore Leads University, Lahore, Pakistan
[b] Hassan II University, Faculty of Sciences Aïn Chock, Laboratory of Mechanics, Casablanca, Morocco
[c] Department of Mathematics, Abdul Wali Khan University, Mardan, 23200, Pakistan
[d] School of Mechanical Engineering, Hanyang University, 222 Wangsimni-ro, Seongdong-gu, Seoul, 04763, South Korea
[e] Department of Industrial Engineering, College of Engineering, King Saud University, P.O. Box 11421, Riyadh, Saudi Arabia

ARTICLE INFO

Keywords:
Free convection flow
Nanofluids
Generalized Atangana-Baleanu derivative
Integral transforms

ABSTRACT

This research looked at the unsteady free convection flows of an incompressible viscous fluid with heat/sink in a vertical cylinder containing a mixture of 47 nm alumina nanoparticles in water. The flow direction is subjected to a perpendicular magnetic field. The generalization entails taking into account a new version of the constitutive equation for thermal flux, known as the generalized Atangana-Baleanu derivative, which is based on the generalized time-fractional derivative with Mittag-Leffler kernel. Using the Laplace transform and the finite Hankel transform, closed forms of analytical solutions for temperature and velocity fields, represented with Bessel and generalized G–function of Lorenzo and Hartley functions, are determined. The generalized solutions are appropriate for particularizations to yield solutions corresponding to fractional derivatives with power-law kernel and exponential kernel. The Mittag-Leffler function is a one-parametric function. It is also possible to acquire the usual situation, which corresponds to classical Fourier's law. To compare models based on generalized Atangana-Baleanu, Atangana-Baleanu, Caputo, and Caputo-Fabrizio time fractional derivatives, numerical simulations produced with the program Mathcad are carried out and visually depicted.

1. Introduction

Any material that may transform or move from one form to another while keeping or holding the capacity to flow is said to be a fluid. Some fluid categories include Newtonian fluid, viscoelastic fluid, and nonlinear relationship between shear stress and shear strain due to either time-independent or time-dependent viscosity. The scientific reality that there is no fluid flow in which shear stress is proportionate to rate of deformation is no longer valid.

In the cylinder, the Coriolis force causes liquids and gases to deflect to the right. The Coriolis force is equally as significant as the

* Corresponding author.
E-mail addresses: nehadali199@yahoo.com (N.A. Shah), abderrahim.wakif-etu@etu.univh2c.ma (A. Wakif), rasoolshahawkum@gmail.com (R. Shah), ysjnuri@hanyang.ac.kr (S.-J. Yook), bsalah@ksu.edu.sa (B. Salah), yasirmahsud16@gmail.com (Y. Mahsud), kashifkingkhankhan@gmail.com (K. Hussain).

https://doi.org/10.1016/j.csite.2021.101518
Received 2 August 2021; Received in revised form 21 September 2021; Accepted 28 September 2021
Available online 2 October 2021

magnetohydrodynamic forces, inertial forces, and viscous forces in the fundamental flow equations. On any fluid flow on the earth's surface, gravitational force, frictional force, centrifugal force, and pressure gradient force all act. The Coriolis force does not affect all transport mechanisms in the atmosphere or the water. The Coriolis force, according to Debnath [1] and Deng et al. [2], can impact transport phenomena on the earth's surface. As a result, it is unrealistic to believe that the Coriolis force has no effect on non-static transport phenomena on Earth's surface. In addition to the Coriolis effect, the earth's rotation is a major contributor to climatic variations on the planet. The Coriolis force may be used to explain the spinning directions of hurricanes, typhoons, tropical cyclones, and strong cyclonic storms. Photobioreactors, sewage treatment, and bio-reactors for specific tissues are all examples of Coriolis force applications in industry; see Refs. [1,2]. Du and Selig [3] provided an analysis of an incompressible constant momentum integral boundary layer ow in three dimensions, with a focus on the importance of rotation as it applies to wind turbine blades.

With several engineering applications, natural convection flow of viscous incompressible fluids in heated horizontal/vertical plates and horizontal/vertical cylinders is a major challenge. As they travel through the environment, hot filaments, also known as vertical cylinders in the glass and polymer sectors, cool. Researchers are interested in the unsteady free convection flow of incompressible fluids in a heated vertical cylinder because of its many applications in physical sciences and engineering. Several scholars have studied fluid flow over vertical cylinders under various physical conditions. As a result, various theoretical, experimental, and computational studies on the flow and heat transfer characteristics of circular cylinders have been carried out, giving many results See Refs. [4–6] and their references.

Choi and Eastman [7] used the term "nanofluid" to describe fluid substances appropriately mixed with particles having diameters in the nanometer 10^{-9} m range. Because they have a significant surface-area-to-volume ratio, particles with a diameter of less than 100 nm have better optical, mechanical, thermal, chemical, magnetic, and electrical characteristics over ordinary solids. Cooling issues and product maintenance may be considered some of the industries' worries because of ever-increasing heat production. Scientists have learned to recognize the unique nature and thermal characteristics of different fluids generated by adding solid particles to save energy and process time (on micrometer and millimeter scales). Nanofluids are used in a variety of sectors, including automobile engine coolants, cancer therapeutics, nanodrug delivery, syphilis detection, and nanofluid detergent (Wong and De Leon [8]). Nguyen et al. [9] performed tests to show how the particle size of water-36nm Al_2O_3, water-47nm Al_2O_3, and water-29nm CuO nanoparticles influences their dynamic viscosity. When particle volume fractions are less than 4%,othe viscosities of both nanofluids containing Al_2O_3 are identical, according to the findings. The viscosity of water-47nm Al_2O_3 nanofluid is significantly greater than that of water-36nm Al_2O_3 nanofluid above this interval. On the case of CuO–H_2O and Al_2O_3–H_2O nanofluids, little is known about the influence of heat sinks in thermal management. As the heat transfer rate rises, Ali et al. [10] explored how to keep the temperature at the base of a heat sink as low as feasible. It was observed that Al_2O_3-water nanofluid had a greater heat transfer rate than CuO-water nanofluid and pure water. Furthermore, the heat sink has the potential to reduce the amount of heat produced by 89.6% between the mini channels.

In recent years, scholars have shown that fractional calculus approaches, such as the theory of non-integer order derivatives and integrals, may successfully describe a variety of phenomena in engineering, bioengineering, physics, and chemistry. Caputo and Mainardi [11], Marks and Hall [12], Olmstead and Handelsman [13], Diethelm and Freed [14], mechanical systems susceptible to damping, Gaul et al. [15], relaxation and reaction kinetics of polymers, Glockle and Nonnenmacher [16], heat conduction, Hristov [17, 18] are some of the important problems modeled with the help of fractional differential operators. Diehelm and colleagues [19] have compiled a helpful set of numerical methods for Caputo-type derivatives, the Riemann-Liouville integral operator, and Mittag-Leffler functions.

MHD is used in a variety of fluid flows and has a wide range of applications, including medication, oil operations, aviation, MHD generators, atomic reactors, and astronomy. Makinde and Animasaun [20] investigated the effects of "autocatalysis compound response and nonlinear Sheikholeslami et al. [21] found MHD nanofluid passing through a penetrable medium with thermal dispersion and heat generation across a vertical plate. Azam et al. [22], who developed solutions for unsteady MHD cross nanofluid flow influenced by nonlinear thermal radiation and zero mass transition conditions, might be incorporated in MHD study. Using Fick's and Fourier's generalized laws, Shao et al. [23] studied the MHD natural convection flow of a viscous fluid with fractional derivatives. Fourier-sine and Laplace integral transformations were used to get the solutions. There are also some current investigations on the relevance of MHD in Refs. [24–29].

This research looked at the unsteady free convection flows of an incompressible viscous fluid with heat/sink in a vertical cylinder containing a mixture of 47 nm alumina nanoparticles in water. The flow direction is subjected to a perpendicular magnetic field. The generalization entails taking into account a new version of the constitutive equation for thermal flux, known as the generalized Atangana-Baleanu derivative, which is based on the generalized time-fractional derivative with Mittag-Leffler kernel. Using the Laplace transform and the finite Hankel transform, closed forms of analytical solutions for temperature and velocity fields, represented with Bessel and generalized G–function of Lorenzo and Hartley functions, are determined. The generalized solutions are appropriate for particularizations to yield solutions corresponding to fractional derivatives with power-law kernel and exponential kernel. The Mittag-Leffler function is a one-parametric function. It is also possible to acquire the usual situation, which corresponds to classical Fourier's law. To compare models based on generalized Atangana-Baleanu, Atangana-Baleanu, Caputo, and Caputo-Fabrizio time fractional derivatives, numerical simulations produced with the program Mathcad are carried out and visually depicted. warm radiation on MHD nanofluid flow through the upper surface" of a paraboloid of disturbance.

2. Preliminary mathematics

The essential mathematical parts of the two-parametric Mittag-Leffler functions and the generalized time-fractional Atangana-

Baleanu derivatives are presented in this section. The next portions of this work will require these mathematical concepts.

2.1. One-parametric and two-parametric Mittag-Leffler functions

The Mittag-Leffler function is a one-parametric function that is defined as [30,31].

$$E_{\vartheta}(z)=\sum_{j=0}^{\infty}\frac{z^{j}}{\Gamma(\vartheta j+1)},\ \ \vartheta>0 \tag{1}$$

where, $\Gamma(\varsigma)=\int_{0}^{\infty}\mathrm{e}^{-\tau}\tau^{\varsigma-1}d\tau,\ \ \mathrm{Re}(\varsigma)>0$ is Euler integral of the second kind.

The two-parametric Mittag-Leffler function generalizes the function $E_{\vartheta}(z)$ and is defined by

$$E_{\vartheta,\varepsilon}(z)=\sum_{j=0}^{\infty}\frac{z^{j}}{\Gamma(\vartheta j+\varepsilon)},\ \ \vartheta>0,\ \ \varepsilon\in\mathbb{C} \tag{2}$$

It is easy to notice that function (1) is a particular case of function (2), so we have

$$E_{\vartheta}(z)=E_{\vartheta,1}(z) \tag{3}$$

Let's recall some properties of Mittag-Leffler functions.

$$\begin{aligned}&E_{\vartheta,\varepsilon}(z)=zE_{\vartheta,\ \vartheta+\varepsilon}(z)+1/\Gamma(\varepsilon),\\&E_{\vartheta,\varepsilon}(z)=\varepsilon E_{\vartheta,1+\varepsilon}(z)+\vartheta z\frac{d}{dz}E_{\vartheta,1+\varepsilon}(z),\end{aligned} \tag{4}$$

$$t^{\gamma}E_{1,1+\gamma}(at)=t^{\gamma}\sum_{j=0}^{\infty}\frac{(at)^{j}}{\Gamma(j+1+\gamma)}=E_{t}(\gamma,a)\ \ -\ \text{the Miller}-\text{Ross function}, \tag{5}$$

$$t^{\gamma}E_{1+\gamma,1+\gamma}\left(at^{1+\gamma}\right)=t^{\gamma}\sum_{j=0}^{\infty}\frac{a^{j}t^{(1+\gamma)j}}{\Gamma[(1+\gamma)(1+j)]}=R_{t}(\gamma,a)\ \ -\ \text{the Robotnov function}, \tag{6}$$

$$\begin{aligned}&\int_{0}^{z}t^{\varepsilon-1}E_{\vartheta,\varepsilon}(bt^{\vartheta})dt=z^{\varepsilon}E_{\vartheta,\varepsilon+1}(bz^{\vartheta}),\ \ \varepsilon>0,\\&\int_{0}^{z}t^{\varepsilon-1}(z-t)^{\gamma-1}E_{\vartheta,\varepsilon}(bt^{\vartheta})dt=z^{\varepsilon+\gamma-1}E_{\vartheta,\varepsilon+\gamma}(bz^{\vartheta})\Gamma(\vartheta),\ \ \varepsilon>0,\ \ \gamma>0,\\&\int_{0}^{z}(z-t)^{\varepsilon-1}e^{bt}dt=z^{\varepsilon}E_{1,\varepsilon+1}(bz)\Gamma(\varepsilon),\ \ \varepsilon>0\end{aligned} \tag{7}$$

The following special form of the one-parametric Mittag-Leffler function [32].

$$G(t-\tau)=E_{\vartheta}\left[-\left(\frac{t-\tau}{\gamma}\right)^{\vartheta}\right],\vartheta\in(0,1),\gamma>0,\tau\in[0,t], \tag{8}$$

along with its derivative

$$M\left(t-\tau\right)=\frac{\partial G(t-\tau)}{\partial\tau}=\frac{-1}{t-\tau}E_{\vartheta,0}\left[-\left(\frac{t-\tau}{\gamma}\right)^{\vartheta}\right],\vartheta\in\left(0,1\right),\gamma>0,\tau\in\left[0,t\right), \tag{9}$$

have applications in the theory of fractional-order viscoelasticity and in some problems modeled by fractional differential equations with constant coefficients.

In the reference [32], some numerical approaches for determining numerical values of Mittag-Leffler functions are described. These methods are based on Mittag-Leffler functions' integral representations. The following integral representations will be used in this paper:

If $\vartheta\in(0,1],\ \ \varepsilon\in\mathbb{R},\ \ 0<\rho<|z|,\ \ |\arg z|>\vartheta\pi,\ \ z\neq0$, then

$$
\begin{aligned}
&E_{\vartheta,\varepsilon}(z) = \int_{\rho}^{\infty} K(\vartheta,\varepsilon,x,z)dx + \int_{-\vartheta\pi}^{\vartheta\pi} P(\vartheta,\varepsilon,\rho,y,z)dy,\\
&K(\vartheta,\varepsilon,x,z) = \frac{1}{\pi\vartheta}x^{\frac{1-\varepsilon}{\vartheta}}\exp\left(-x^{1/\vartheta}\right)\frac{x\sin(\pi(1-\varepsilon)) - z\sin(\pi(1-\varepsilon+\vartheta))}{x^2 - 2xz\cos(\pi\vartheta) + z^2},\\
&P(\vartheta,\varepsilon,\rho,y,z) = \frac{\rho^{1+(1-\varepsilon)/\vartheta}}{2\pi\vartheta}\frac{\exp\left(\rho^{1/\vartheta}\cos(y/\vartheta)\right)\exp(i\varphi)}{\rho\exp(iy) - z},\\
&\varphi = \rho^{1/\vartheta}\sin(y/\vartheta) + y(1 + (1-\varepsilon)/\vartheta).
\end{aligned}
\tag{10}
$$

The integral representation

$$
\int_0^{\infty} e^{-st}t^{m\alpha}E_{\vartheta}^{(m)}(\pm bt^{\vartheta})dt = \frac{m!s^{\vartheta-1}}{(s^{\vartheta}\mp b)^{m+1}},\quad \mathrm{Re}(s) > 0,\quad \mathrm{Re}(\vartheta) > 0,\quad m \in \mathbb{N}
\tag{11}
$$

coupled with the definition of the Laplace transform of a function $\Psi(t)$, $L\{\Psi(t)\} = \int_0^{\infty}\Psi(t)\exp(-st)dt$ ogive the following relationship:

$$
L\left\{t^{m\alpha}E_{\vartheta}^{(m)}(\pm bt^{\vartheta})\right\} = \frac{m!s^{\vartheta-1}}{(s^{\vartheta}\mp b)^{m+1}},\quad \mathrm{Re}(s) > 0,\quad \mathrm{Re}(\vartheta) > 0,\quad m \in \mathbb{N}
\tag{12}
$$

In this particular instance, $m = 0$, Eq. (12) becomes

$$
L\{E_{\vartheta}(\pm bt^{\vartheta})\} = \frac{s^{\vartheta-1}}{s^{\vartheta}\mp b}
\tag{13}
$$

2.2. Generalized Atangana-Baleanu time-fractional derivative

The function

$$
\chi(t,\vartheta,\varepsilon) = \frac{1}{1-\vartheta}E_{\varepsilon}\left(\frac{-\vartheta}{1-\vartheta}t^{\varepsilon}\right),\quad t \geq 0,\quad \vartheta \in (0,1),\quad \varepsilon > 0
\tag{14}
$$

is called the generalized Atangana-Baleanu kernel.

The Laplace transform of the kernel (14) is given by

$$
L\{\chi(t,\vartheta,\varepsilon)\} = \frac{s^{\varepsilon-1}}{(1-\vartheta)s^{\varepsilon} + \vartheta}
\tag{15}
$$

Using the Laplace transform, the following properties of the generalized Atangana-Baleanu kernel (14) are found:

$$
\begin{aligned}
&\lim_{\vartheta\to 0}L\{\chi(t,\vartheta,\varepsilon)\} = L\left\{\lim_{\vartheta\to 0}\chi(t,\vartheta,\varepsilon)\right\} = \frac{s^{\varepsilon-1}}{s^{\varepsilon}} = L\{1\},\\
&\lim_{\vartheta\to 1}L\{\chi(t,\vartheta,\varepsilon)\} = L\left\{\lim_{\vartheta\to 1}\chi(t,\vartheta,\varepsilon)\right\} = \frac{1}{s^{1-\varepsilon}} = L\left\{\frac{t^{-\varepsilon}}{\Gamma(1-\varepsilon)}\right\} = L\{\chi_0(t,\varepsilon)\},\\
&\lim_{\varepsilon\to 0}L\{\chi(t,\vartheta,\varepsilon)\} = L\left\{\lim_{\varepsilon\to 0}\chi(t,\vartheta,\varepsilon)\right\} = \frac{1}{s} = L\{1\},\\
&\lim_{\varepsilon\to 1}L\{\chi(t,\vartheta,\varepsilon)\} = L\left\{\lim_{\varepsilon\to 1}\chi(t,\vartheta,\varepsilon)\right\} = \frac{1}{(1-\vartheta)s + \vartheta} = L\left\{\frac{1}{1-\vartheta}e^{\frac{-\vartheta t}{1-\vartheta}}\right\} = L\{\chi_1(t,\vartheta)\},
\end{aligned}
\tag{16}
$$

therefore,

$$\begin{aligned}
&\lim_{\vartheta\to 0}\chi(t,\vartheta,\varepsilon) = \lim_{\varepsilon\to 0}\chi(t,\vartheta,\varepsilon) = 1,\\
&\lim_{\vartheta\to 1}\chi(t,\vartheta,\varepsilon) = \chi_0(t,\varepsilon) = \frac{t^{-\vartheta}}{\Gamma(1-\vartheta)},\\
&\lim_{\varepsilon\to 1}\chi(t,\vartheta,\varepsilon) = \chi_1(t,\vartheta) = \frac{1}{1-\vartheta}\exp\Big(\frac{-\vartheta t}{1-\vartheta}\Big),\\
&\chi(t,\vartheta,\vartheta) = \chi_2(t,\vartheta) = \frac{1}{1-\vartheta}E_\vartheta\Big(-\frac{\vartheta}{1-\vartheta}t^\vartheta\Big),\\
&\lim_{\substack{\vartheta\to 1\\ \varepsilon\to 1}}\chi(t,\vartheta,\varepsilon) = \delta(t).
\end{aligned} \tag{17}$$

In the above relations, functions $\chi_0(t,\vartheta)$, $\chi_1(t,\vartheta)$, $\chi_2(t,\vartheta)$ and $\delta(t)$ are, respectively Caputo kernel, Caputo-Fabrizio kernel, Atangana-Baleanu kernel, and the Dirac's distribution.

Definition (The generalized Atangana-Baleanu fractional derivative in Caputo sense). If $f\in H^1(0,T)$, $T>0$, $\vartheta\in[0,1]$, $\varepsilon\in[0,1]$, the generalized Atangana-Baleanu fractional derivative in Caputo sense, of order α of the function $f(t)$ is defined by the relation,

$$\left({}^{GAB}D_t^{\vartheta,\varepsilon}f\right)(t) = \chi(t,\vartheta,\varepsilon) * \dot{f}(t) = \int_0^t \chi(t-\tau,\vartheta,\varepsilon)\dot{f}(\tau)d\tau \tag{18}$$

Using Eqs. (17) and (18), we obtain the following properties of the generalized Atangana-Baleanu time-fractional derivative:

$$\left({}^{GAB}D_t^{0,\varepsilon}f\right)(t) = \left({}^{GAB}D_t^{\vartheta,0}f\right)(t) = 1 * \dot{f}(t) = \int_0^t \dot{f}(\tau)d\tau = f(t) - f(0), \tag{19}$$

$$\left({}^{GAB}D_t^{1,1}f\right)(t) = \delta(t) * \dot{f}(t) = \dot{f}(t) = \frac{df(t)}{dt}, \tag{20}$$

$$\left({}^{GAB}D_t^{1,\varepsilon}f\right)(t) = \chi_0(t,\varepsilon) * \dot{f}(t) = \left({}^{C}D_t^{\varepsilon}f\right)(t) \tag{21}$$

$$\left({}^{GAB}D_t^{\vartheta,1}f\right)(t) = \chi_1(t,\varepsilon) * \dot{f}(t) = \left({}^{CF}D_t^{\varepsilon}f\right)(t) \tag{22}$$

$$\left({}^{GAB}D_t^{\vartheta,\vartheta}f\right)(t) = \chi_2(t,\vartheta) * \dot{f}(t) = \left({}^{AB}D_t^{\vartheta}f\right)(t) \tag{23}$$

where, $({}^{C}D_t^{\varepsilon}f)(t)$ denotes the time-fractional Caputo derivative, $({}^{CF}D_t^{\varepsilon}f)(t)$ is time-fractional Caputo-Fabrizio derivative, and $({}^{AB}D_t^{\vartheta}f)(t)$ denotes the time-fractional Atangana-Baleanu derivative.

Associated with the generalized Atangana-Baleanu derivative, we define the following fractional integral operator:

$$\left(J_t^{\vartheta,\varepsilon}f\right)(t) = (1-\vartheta)f(t) + \vartheta\psi_0(t,\varepsilon) * f(t), \quad \vartheta\in[0,1], \quad \varepsilon\in(0,1], \tag{24}$$

where the kernel $\psi_0(t,\varepsilon)$ is defined as

$$\psi_0(t,\varepsilon) = \frac{t^{\varepsilon-1}}{\Gamma(\varepsilon)} \tag{25}$$

It is observed that $L\{\psi_0(t,\varepsilon)\} = \frac{1}{s^\varepsilon}$, $\lim_{\varepsilon\to 0} L\{\psi_0(t,\varepsilon)\} = 1 = L\{\delta(t)\}$, therefore,

$$\lim_{\varepsilon\to 0}\psi_0(t,\varepsilon) = \delta(t) \tag{26}$$

Using the property (26), the fractional integral operator can be defined for $\varepsilon = 0$.

The fractional integral operator (24) has the following properties:

$$\begin{aligned}
&\left(J_t^{1,0}f\right)(t) = \delta(t) * f(t) = f(t),\\
&\left(J_t^{1,1}f\right)(t) = 1 * f(t) = \int_0^t f(\tau)d\tau.
\end{aligned} \tag{27}$$

Regarding the generalized Atangana-Baleanu derivative and associated fractional integral operator, we remember the proposition:

Proposition. The following relationships are fulfilled:

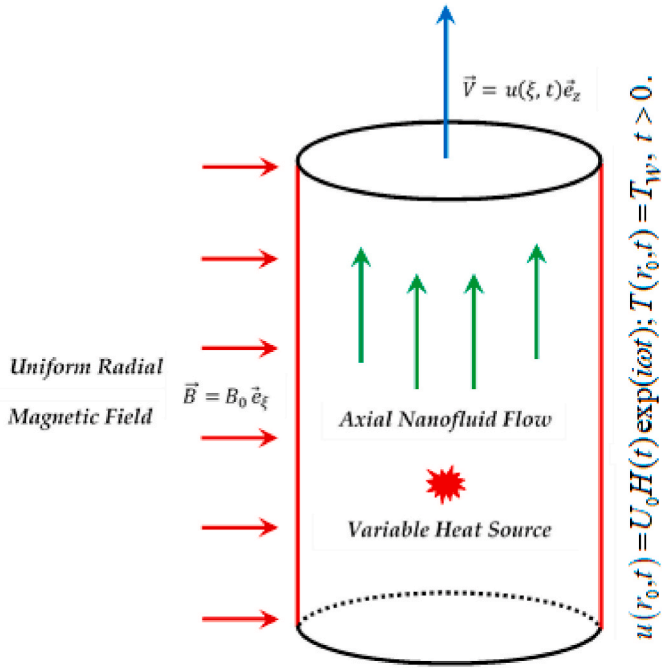

Fig. 1. Flow geometry.

$$\begin{aligned}\left({}^{GAB}D_t^{\vartheta,\varepsilon}\left(J_t^{\vartheta,\varepsilon}f\right)\right)(t) &= f(t) - (1-\vartheta)f(0)\chi(t,\vartheta,\varepsilon),\\ \left(J_t^{\vartheta,\varepsilon}\left({}^{GAB}D_t^{\vartheta,\varepsilon}f\right)\right)(t) &= f(t) - f(0).\end{aligned} \tag{28}$$

The demonstration of the above proposition can be found in the reference [33].
The generalized fractional integral operator (24) contains the following particular cases:

$\vartheta = 1,\ \ \varepsilon \in [0,1],$

$$1^0\left(J_t^{1,\varepsilon}f\right)(t) = \psi_0(t,\varepsilon)*f(t) = \frac{1}{\Gamma(\varepsilon)}\int_0^t (t-\tau)^{\varepsilon-1}f(\tau)d\tau, \tag{29}$$

i.e. the well-known Riemann-Liouville fractional integral operator.

$\vartheta \in [0,1],\ \ \varepsilon = 1,$

$$2^0.\left(J_t^{\vartheta,1}f\right)(t) = (1-\vartheta)f(t) + \vartheta\int_0^t f(\tau)d\tau, \tag{30}$$

that is the integral operator associated to the Caputo-Fabrizio derivative.

$\vartheta = \varepsilon \in [0,1],$

$$3^0\ \left(J_t^{\vartheta,\vartheta}f\right)(t) = (1-\vartheta)f(t) + \frac{\vartheta}{\Gamma(\vartheta)}\int_0^t (t-\tau)^{\vartheta-1}f(\tau)d\tau, \tag{31}$$

that is the fractional integral operator associated with Atangana-Baleanu fractional derivative.

3. Mathematical formulation and solution of the problem

Consider transient free convection flow of an incompressible viscous fluid in an infinite vertical cylinder of radius r_0. The z-axis is considered along the axis of cylinder in vertical upward direction and the radial coordinate r is taken normal to it. Initially at time $t \leq 0$, it is assumed that the cylinder is at rest and the cylinder and fluid are at the same temperature T_∞. After time $t = 0$, the cylinder begins to oscillate along its axis and induces the motion in the fluid with velocity $U_0H(t)\exp(i\omega t)$, where U_0 is the characteristic velocity, $H(t)$ is the unit step function and ω is the frequency of oscillation. At the same time, the cylinder temperature raised to T_w which is thereafter maintained constant (see Fig. 1).

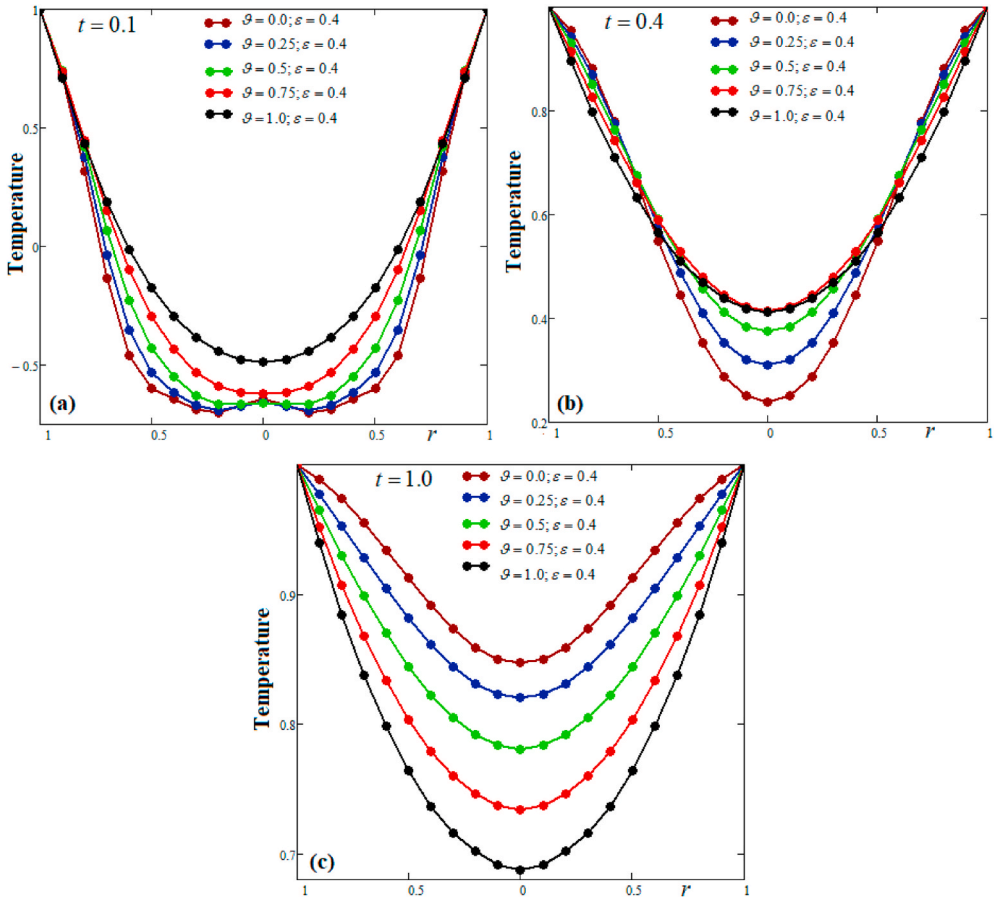

Fig. 2. Profile of temperature versus r for ϑ variation at different values of time t.

We assume that the velocity and temperature are the function of ξ and t only. For such a flow, the constraint of incompressibility is identically satisfied. It is also assumed that all the fluid properties are constant except for the density in the buoyancy term, which is given by the usual Boussinesq's approximation. Under these assumptions, a well-defined problem is modeled in terms of the following partial differential equations:

$$\rho_{nf}\frac{\partial u(\xi,t)}{\partial t}=\mu_{nf}\frac{1}{\xi}\frac{\partial}{\partial \xi}\left(\xi\frac{\partial u(\xi,t)}{\partial \xi}\right)+g(\rho\beta_T)_{nf}[T(\xi,t)-T_\infty]-\sigma_{nf}B_0^2u\left(\xi,t\right), \tag{32}$$

$$\left(\rho c_p\right)_{nf}\frac{\partial T(\xi,t)}{\partial t}=-\left(\frac{\partial}{\partial \xi}+\frac{1}{\xi}\right)q(\xi,t)-Q[T(\xi,t)-T_\infty], \tag{33}$$

$$q(\xi,t)=-k_{nf}\frac{\partial T(\xi,t)}{\partial \xi}. \tag{34}$$

here $T(\xi,t)$ is the fluid temperature, $q(\xi,t)$ is the thermal flux, g is the acceleration due to the gravity, ρ_{nf} is the density of the nanofluid, β_{nf} is the thermal expansion coefficient of the nanofluid, μ_{nf} is the dynamic viscosity of the nanofluid, $(c_p)_{nf}$ is the specific heat of the nanofluid at constant pressure and k_{nf} is the thermal conductivity of the nanofluid. The thermal-physical properties of nanofluid are defined in [34,35].

$$\rho_{nf}=(1-\varphi)\rho_{bf}+\varphi\rho_{np},\ \frac{\mu_{nf}}{\rho_{nf}\nu_{bf}}=\frac{0.904e^{0.148\varphi}}{1-\varphi+\frac{\rho_{np}}{\rho_{bf}}\varphi},$$

$$(\rho\beta)_{nf}=(1-\varphi)(\rho\beta)_{bf}+\varphi(\rho\beta)_{np},\ \left(\rho c_p\right)_{nf}=(1-\varphi)\left(\rho c_p\right)_{bf}+\varphi\left(\rho c_p\right)_{np},$$

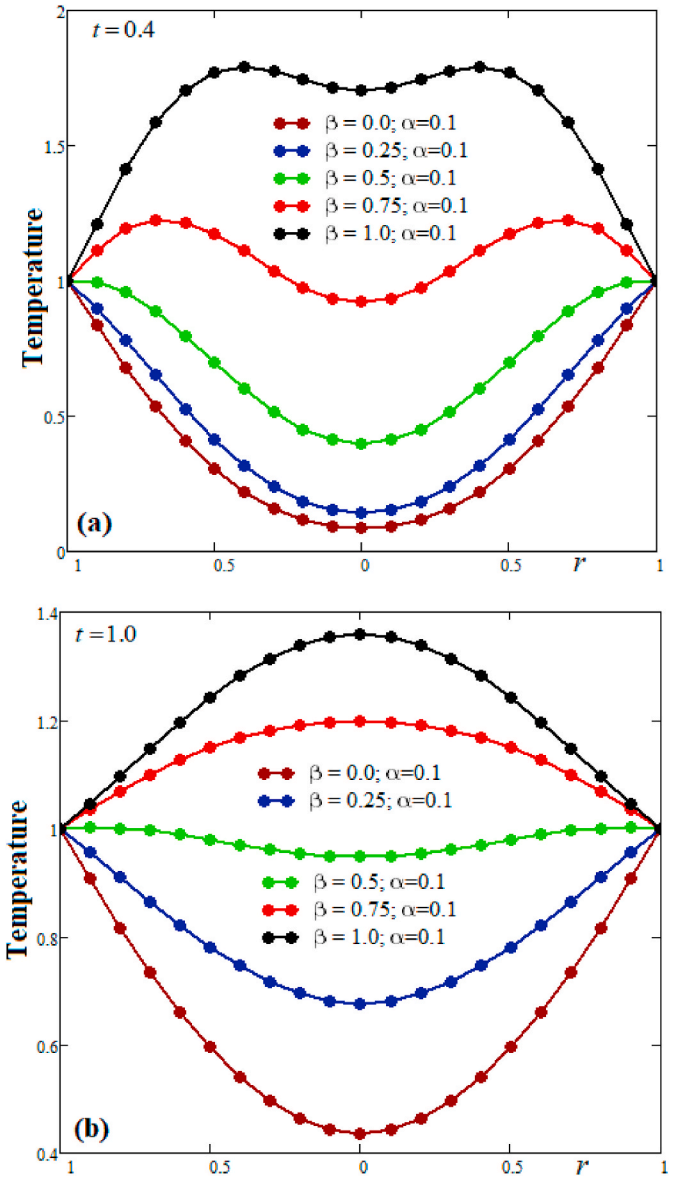

Fig. 3. Profile of temperature versus r for ε variation at different values of time t.

$$\frac{k_{nf}}{k_f}=\frac{k_{np}+2k_{bf}+2\varphi\left(k_{bf}-k_{nf}\right)}{k_{np}+2k_{bf}-\varphi\left(k_{bf}-k_{nf}\right)},\ \frac{\sigma_{nf}}{\sigma_{bf}}=\left(1+\frac{3(\sigma-1)\varphi}{(\sigma+2)-(\sigma-1)\varphi}\right),\ \sigma=\frac{\sigma_s}{\sigma_f},$$

where φ is the nanoparticle volume fraction, the indexes f allude to the fluid, with appropriate initial and boundary conditions:

$$u(\xi,0)=0,\ \ T(\xi,0)=T_\infty\ ;\ \xi\in[0,\ r_0], \tag{35}$$

$$u(r_0,t)=U_0H(t)\exp(i\omega t);\ T(r_0,t)=T_w,\ t>0\ . \tag{36}$$

Let us introduce the following dimensionless variables

$$\xi^*=\frac{\xi}{r_0},\ \Omega=\frac{u}{U_0},\ t^*=\frac{t\nu_{nf}}{r_o^2},\ \Theta^*=\frac{T-T_\infty}{T_w-T_\infty},\ q^*=\frac{q}{q_0},\ q_0=\frac{(T_w-T_\infty)k_{nf}}{r_0},\ Q^*=\frac{Qr_o^2}{k_{nf}} \tag{37}$$

where U_0 is a characteristic velocity. Using the above dimensionless variables and parameters and after dropping out the * notation in Eqs. (32)-(36), owe obtain

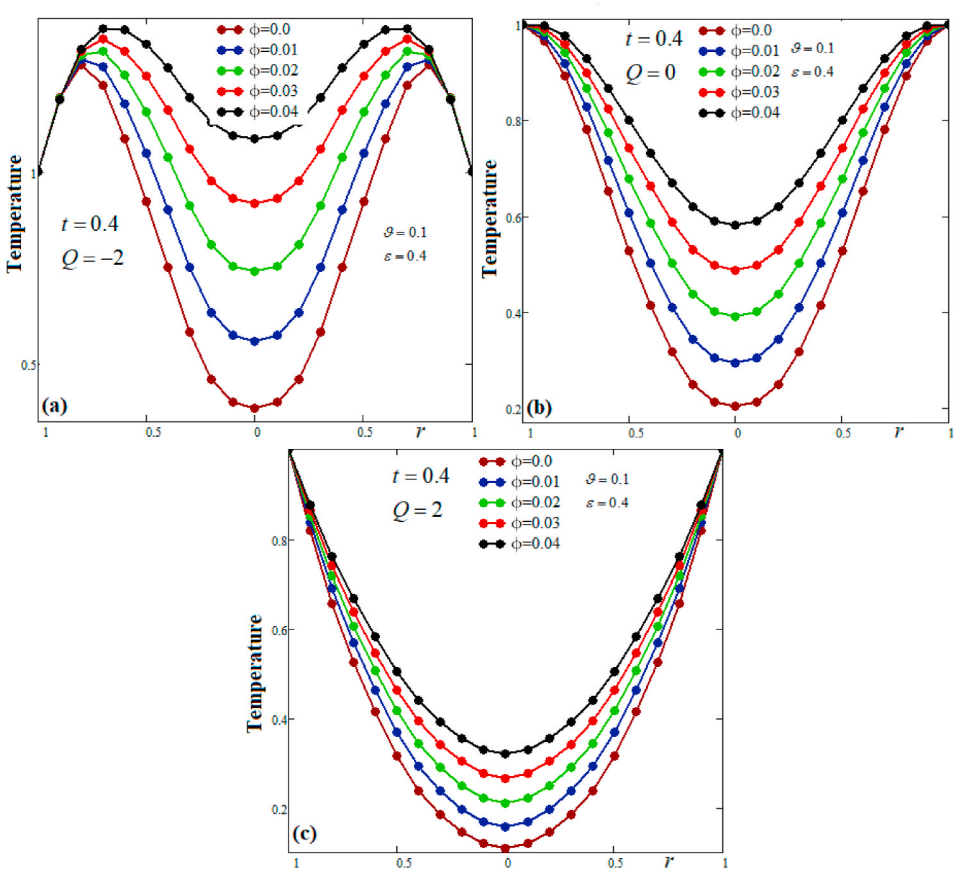

Fig. 4. Profile of temperature versus r for φ variation at different vales of Q.

$$\frac{\partial \Omega(\xi,t)}{\partial t}=\frac{\partial^2 \Omega(\xi,t)}{\partial \xi^2}+\frac{1}{\xi}\frac{\partial \Omega(\xi,t)}{\partial \xi}+Gr\Theta(\xi,t)-M\Omega(\xi,t);\ \xi\in(0,1),\ t>0, \tag{38}$$

$$\frac{\partial \Theta(\xi,t)}{\partial t}=-\frac{1}{\mathrm{Pr}}\left(\frac{\partial}{\partial \xi}+\frac{1}{\xi}\right)q(\xi,t)-Q\Theta(\xi,t), \tag{39}$$

$$q(\xi,t)=-\frac{\partial \Theta(\xi,t)}{\partial \xi}. \tag{40}$$

$$u(\xi,0)=0,\ \ \theta(\xi,0)=0\ ;\ \xi\in[0,\ 1], \tag{41}$$

$$u(1,t)=H(t)\exp(i\omega t);\ \theta(1,t)=1,\ t>0, \tag{42}$$

where $M=B_0R\sqrt{\frac{\sigma_{nf}}{\mu_{nf}}}$ represents the magnetic parameter, $Gr=\frac{g(\beta_T)_{nf}r_0^2(T_w-T_\infty)}{U_0\nu_{nf}}$ is the Grashof number and $\mathrm{Pr}=\frac{(\mu c_p)_{nf}}{k_{nf}}$ is Prandtl number.

The form of the constitutive equations can be changed to define a medium with new attributes in order to explore a new mathematical model. The thermal flux is represented by a time-fractional derivative equation that constitutes an extension of the traditional Fourier's law of heat conduction in the current model as

$$q(\xi,t)=-{}^{GAB}D_t^{\vartheta,\varepsilon}\frac{\partial \Theta(\xi,t)}{\partial \xi}, \tag{43}$$

where ${}^{GAB}D_t^{\vartheta,\varepsilon}$ the generalized Atangana-Baleanu fractional derivative in Caputo sense defined by the relation,

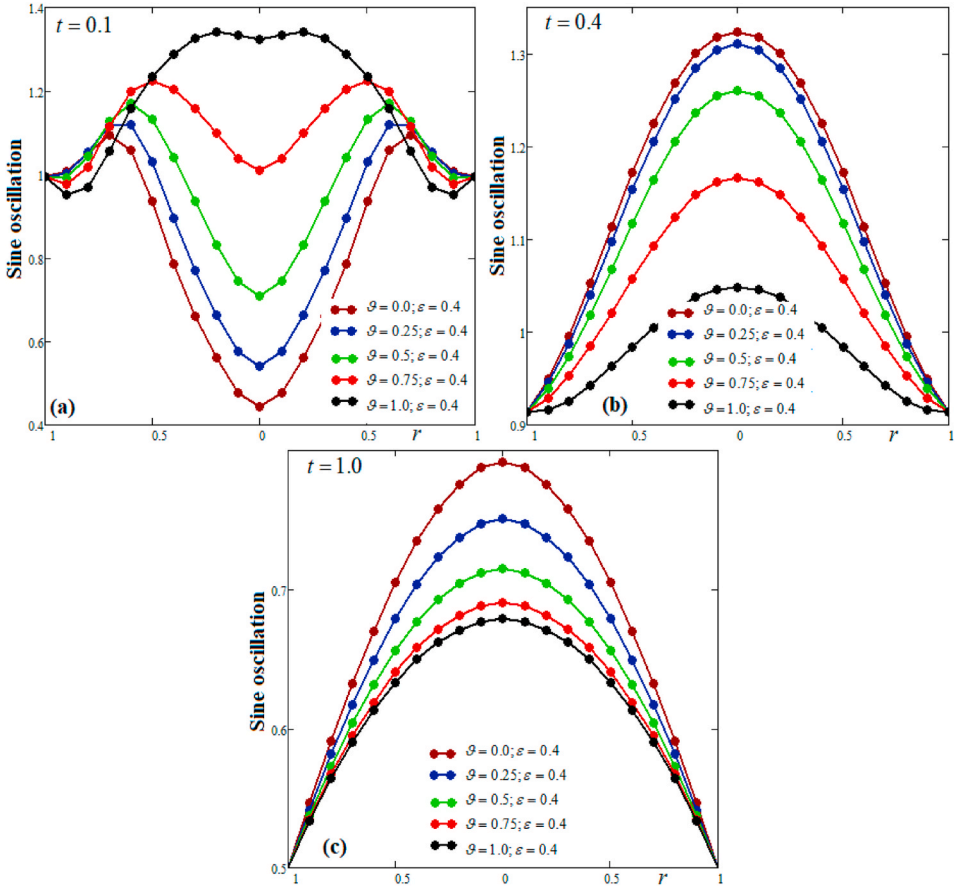

Fig. 5. (i). Profile of velocity profile with sine oscillation versus r for ϑ variation at different vales of time t. Fig. 5(ii). Profile of velocity profile with cosine oscillation versus r for ϑ variation at different values of time t.

$$\left({}^{GAB}D_t^{\vartheta,\varepsilon}f\right)(t) = \chi(t,\vartheta,\varepsilon)*\dot{f}(t) = \int_0^t \chi(t-\tau,\vartheta,\varepsilon)\dot{f}(\tau)d\tau;$$

$$\chi(t,\vartheta,\varepsilon) = \frac{1}{1-\vartheta}E_\varepsilon\left(\frac{-\vartheta}{1-\vartheta}t^\varepsilon\right), \quad t \geq 0, \quad \vartheta \in (0,1), \quad \varepsilon > 0.$$

Using Eq. (43) in Eq. (39), we obtain

$$\frac{\partial\Theta(\xi,t)}{\partial t} = \frac{1}{\mathrm{Pr}}\,{}^{GAB}D_t^{\vartheta,\varepsilon}\left(\frac{\partial^2}{\partial\xi^2}+\frac{1}{\xi}\frac{\partial}{\partial\xi}\right)\Theta(\xi,t) - Q\Theta(\xi,t). \tag{44}$$

4. Solution of the problem

4.1. Temperature distribution

We applied the Laplace transformation to Eqs. (43) and $(39)_2$, we get

$$s\overline{\Theta}(\xi,s) = \left[\frac{s^\varepsilon}{\mathrm{Pr}((1-\vartheta)s^\varepsilon+\vartheta)}\right]\left[\frac{\partial^2\overline{\Theta}(\xi,s)}{\partial\xi^2}+\frac{1}{\xi}\frac{\partial\overline{\Theta}(\xi,s)}{\partial\xi}\right] - Q\overline{\Theta}(\xi,s) \tag{45}$$

$$\overline{\Theta}(1,s) = \frac{1}{s}, \tag{46}$$

where $\overline{\Theta}(\xi,s) = \int_0^\infty \Theta(\xi,t)e^{-st}dt.$

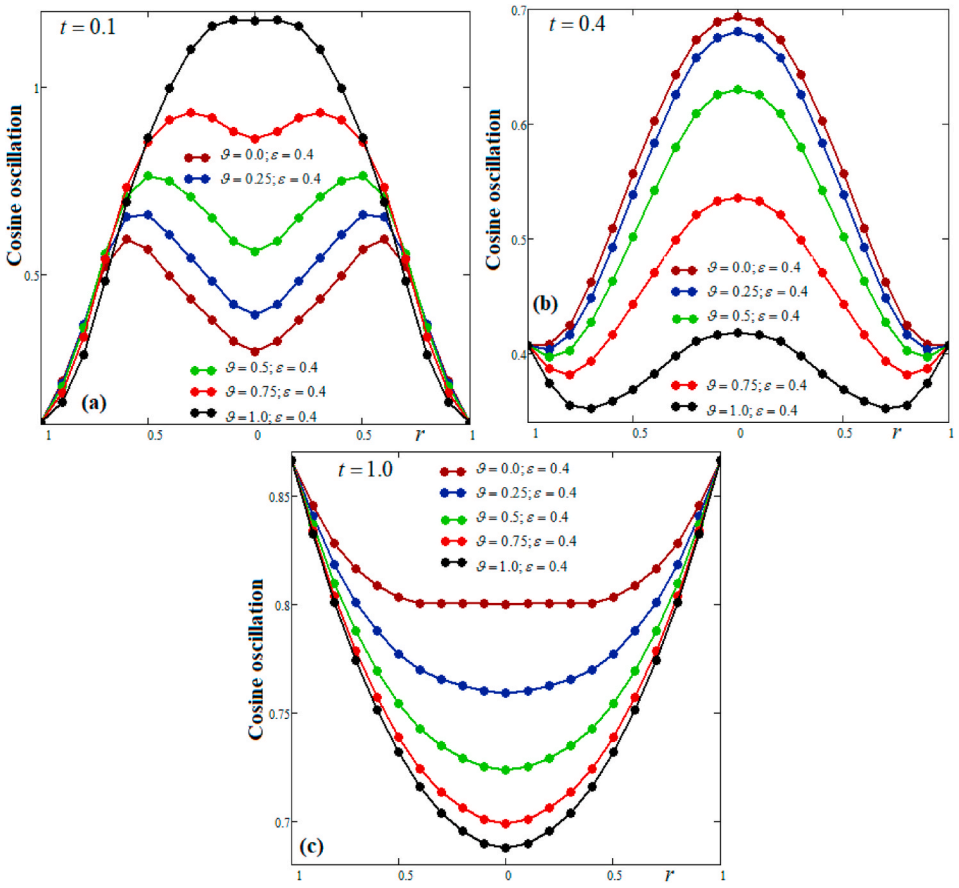

Fig. 5. (*continued*).

We get the following result by applying the finite Hankel transform to Eq. (45) and utilizing the boundary condition in Eq. (46).

$$\overline{\Theta}_H(\xi_n, s) = \frac{\xi_n J_1(\xi_n) s^{\varepsilon-1}}{\Pr(s+Q)((1-\vartheta)s^{\varepsilon}+\vartheta)+\xi_n^2 s^{\varepsilon}}, \tag{47}$$

where $\overline{\Theta}_H(\xi_n, s) = \int_0^1 \overline{\Theta}(\xi, s)\xi J_0(\xi\xi_n)d\xi$ is the finite Hankel transform of function $\overline{\Theta}(\xi, q)$ and ξ_n, n = 1,2 … are the positive roots of the equation $J_0(x) = 0$, J_0 being the Bessel function of the first kind and order zero.

Eq. (47) can be written in the following equivalent form

$$\overline{\Theta}_H(\xi_n, s) = \frac{J_1(\xi_n)}{\xi_n}\frac{1}{s} - \frac{J_1(\xi_n)}{\xi_n}\frac{\Pr(s+Q)((1-\vartheta)s^{\varepsilon}+\vartheta)}{s\left[\Pr(s+Q)((1-\vartheta)s^{\varepsilon}+\vartheta)+\xi_n^2 s^{\varepsilon}\right]}, \tag{48}$$

Applying the inverse Hankel transform to Eq. (17), get

$$\overline{\Theta}(\xi, s) = \frac{1}{s} - 2\sum_{n=1}^{\infty}\frac{J_0(\xi\xi_n)}{\xi_n J_1(\xi_n)}\frac{\Pr(s+Q)((1-\vartheta)s^{\varepsilon}+\vartheta)}{s\left[\Pr(s+Q)((1-\vartheta)s^{\varepsilon}+\vartheta)+\xi_n^2 s^{\varepsilon}\right]}. \tag{49}$$

Using series formula Eq. (49) can be written as

$$\overline{\Theta}(\xi, s) = \frac{1}{s} - 2\sum_{n=1}^{\infty}\frac{J_0(\xi\xi_n)}{\xi_n J_1(\xi_n)}\sum_{k=0}^{\infty}\frac{(-1)^k \xi_n^{2k}}{[\Pr(1-\vartheta)]^k}\left[\frac{s^{-1}}{(s+Q)^k}\frac{s^{\varepsilon k-1}}{\left(s^{\varepsilon}+\frac{\vartheta}{1-\vartheta}\right)^k}\right]. \tag{50}$$

Taking the inverse Laplace transform, we obtain

$$\Theta(\xi, t) = 1 - 2\sum_{n=1}^{\infty}\frac{J_0(\xi\xi_n)}{\xi_n J_1(\xi_n)}\sum_{k=0}^{\infty}\frac{(-1)^k \xi_n^{2k}}{[\Pr(1-\vartheta)]^k}\left[G_{1,-1,\,k}(t, -Q) * G_{\varepsilon,\varepsilon k-1,\,k}\left(t, -\frac{\vartheta}{1-\vartheta}\right)\right]. \tag{51}$$

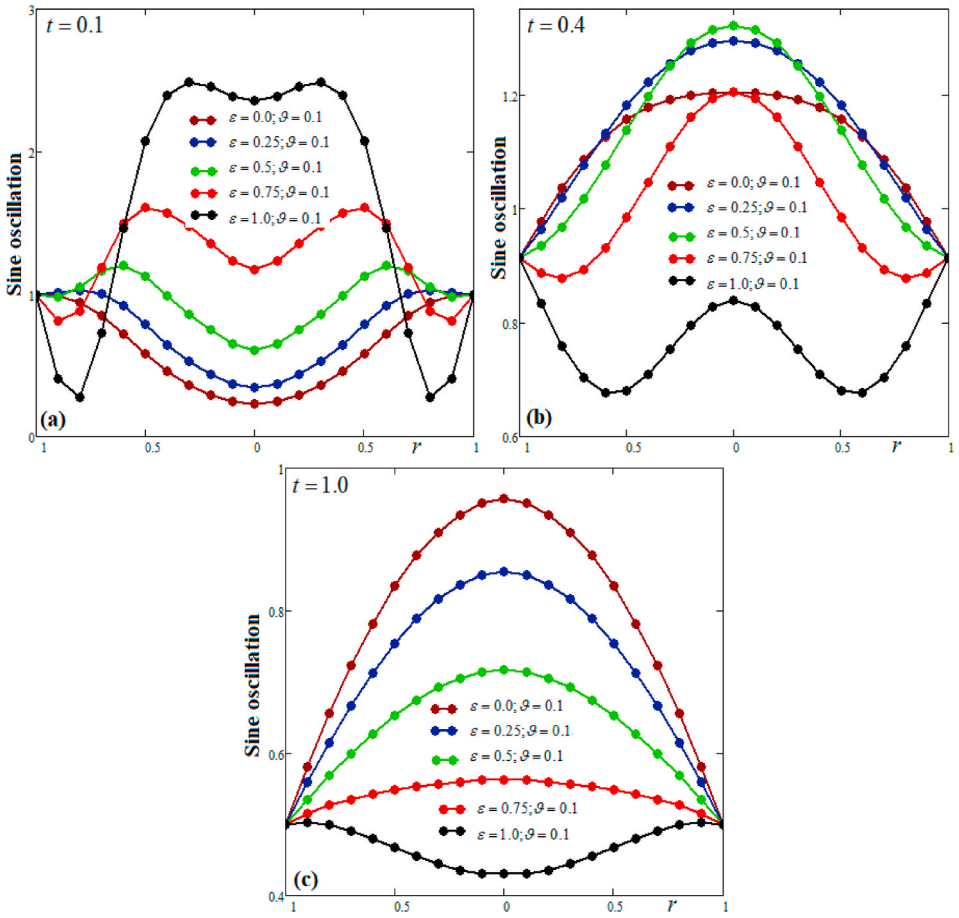

Fig. 6. (i). Profile of velocity profile with sine oscillation versus r for ε variation at different vales of time t. Fig. 6(ii). Profile of velocity profile with cosine oscillation versus r for ε variation at different vales of time t.

$G_{a,\,b,\,c}(t,d) = L^{-1}\left\{\frac{s^b}{(s^a-d)^c}\right\}$, $R(s) > 0$, $R(ac-b) > 0$, $\left|\frac{d}{s^a}\right| < 1$, is the generalized G–function of Lorenzo and Hartley.

For classical case $\vartheta = 1$ and $\varepsilon = 0$, we get ordinary model of temperature distribution as

$$\begin{aligned}\Theta(\xi,t) &= 1 - 2\sum_{n=1}^{\infty}\frac{J_0(\xi\xi_n)}{\xi_n J_1(\xi_n)}\sum_{k=0}^{\infty}\frac{(-1)^k\xi_n^{2k}}{\mathrm{Pr}^k}\left[G_{1,-1,\,k}(t,-Q)*H(t)\right]\\ &= 1 - 2\sum_{n=1}^{\infty}\frac{J_0(\xi\xi_n)}{\xi_n J_1(\xi_n)}\sum_{k=0}^{\infty}\frac{(-1)^k\xi_n^{2k}}{\mathrm{Pr}^k}\left[\int_0^t G_{1,-1,\,k}(\tau,-Q)d\tau\right].\end{aligned} \tag{52}$$

4.2. Velocity field

Taking Laplace transformation of Eqs. (38) and $(42)_1$, we obtain

$$s\overline{\Omega}(\xi,s) = \frac{\partial^2\overline{\Omega}(\xi,s)}{\partial\xi^2} + \frac{1}{\xi}\frac{\partial\overline{\Omega}(\xi,s)}{\partial\xi} + Gr\overline{\Theta}(\xi,s) - M\overline{\Omega}(\xi,s), \tag{53}$$

$$\overline{\Omega}(1,s) = \frac{1}{s-i\omega}, \tag{54}$$

where $\overline{\Omega}(\xi,s) = \int_0^{\infty}\Omega(\xi,t)e^{-st}dt.$

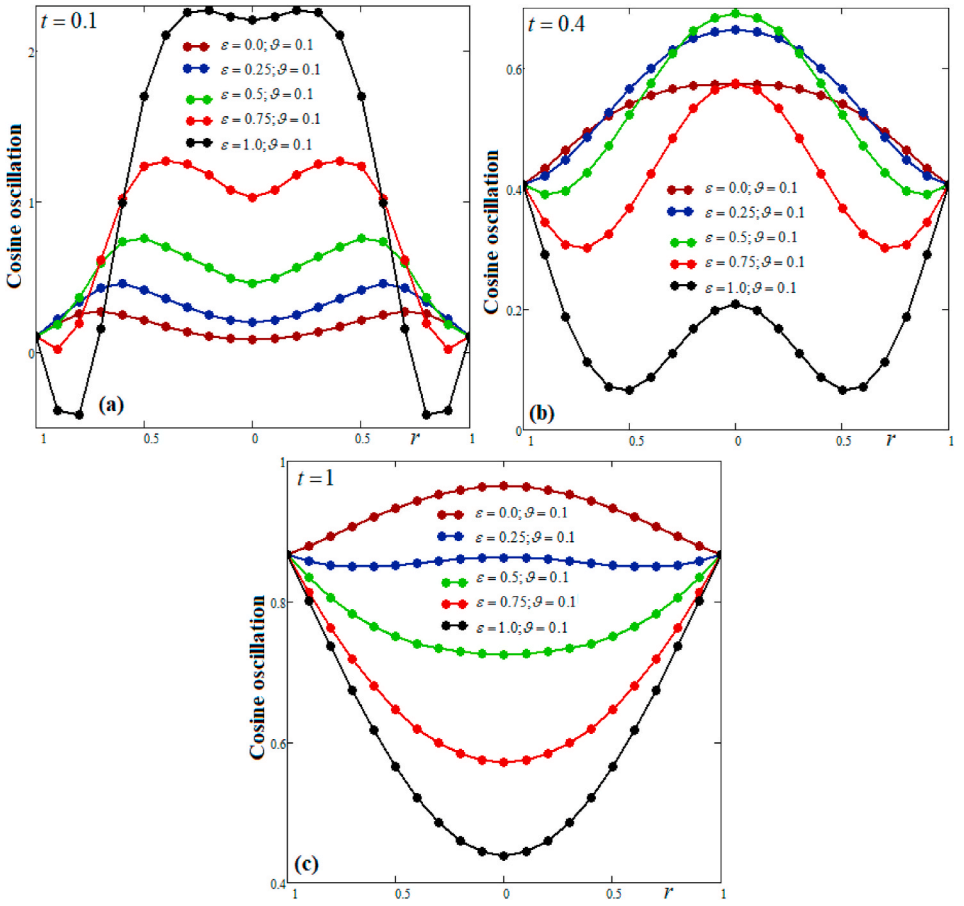

Fig. 6. (*continued*).

Applying finite Hankel transform to Eq. (53) and using boundary condition in Eq. (54) and Eq. (47), we obtain

$$\overline{\Omega}_H(\xi_n,s)=\frac{\xi_n J_1(\xi_n)}{(s-i\omega)\left(s+\xi_n^2+M\right)}+\frac{Gr\xi_n J_1(\xi_n)s^{\varepsilon-1}}{\Pr(s+Q)((1-\vartheta)s^{\varepsilon}+\vartheta)+\xi_n^2 s^{\varepsilon}}\frac{1}{s+\xi_n^2+M}, \tag{55}$$

where $\overline{\Omega}_H(\xi_n,s)=\int_0^1 \overline{\Omega}(\xi,s)\xi J_0(\xi\xi_n)d\xi$ is the finite Hankel transform of function $\overline{u}(\xi,q)$ and ξ_n, n = 1,2 … are the positive root of the equation $J_0(x)=0$, oJ_0 being the Bessel function of the first kind and order zero.

Eq. (55) can be written in the following equivalent form

$$\begin{aligned}\overline{\Omega}_H(\xi_n,s)=&\frac{J_1(\xi_n)}{\xi_n}\frac{1}{s-i\omega}-\frac{J_1(\xi_n)}{\xi_n}\left[1-\frac{\xi_n^2}{s+\xi_n^2+M}\right]\frac{1}{s-i\omega}+\\&+Gr\xi_n J_1(\xi_n)\sum_{k=0}^{\infty}\frac{(-1)^k\xi_n^{2k}}{\Pr^{k+1}(1-\vartheta)^{k+1}}\frac{s^{-1}}{(s+Q)^{k+1}}\frac{s^{\varepsilon(k+1)}}{\left(s^{\varepsilon}+\frac{\vartheta}{1-\vartheta}\right)^{k+1}}\frac{1}{s+\xi_n^2+M}.\end{aligned} \tag{56}$$

Applying inverse Laplace transform to Eq. (56), we obtain

$$\begin{aligned}\widetilde{\Omega}_H(\xi_n,t)=&\frac{J_1(\xi_n)}{\xi_n}H(t)e^{i\omega t}-\frac{J_1(\xi_n)}{\xi_n}\left[\delta(t)-\xi_n^2 e^{-\left(\xi_n^2+M\right)t}\right]*H(t)e^{i\omega t}+\\&+Gr\xi_n J_1(\xi_n)\sum_{k=0}^{\infty}\frac{(-1)^k\xi_n^{2k}}{\Pr^{k+1}(1-\vartheta)^{k+1}}G_{1,-1,\,k+1}(t,-Q)*G_{\varepsilon,\varepsilon(k+1),\,k+1}\left(t,-\frac{\vartheta}{1-\vartheta}\right)*e^{-\left(\xi_n^2+M\right)t},\end{aligned} \tag{57}$$

here * represent the convolution product.

Taking inverse Hankel transform of Eq. (57), we obtain

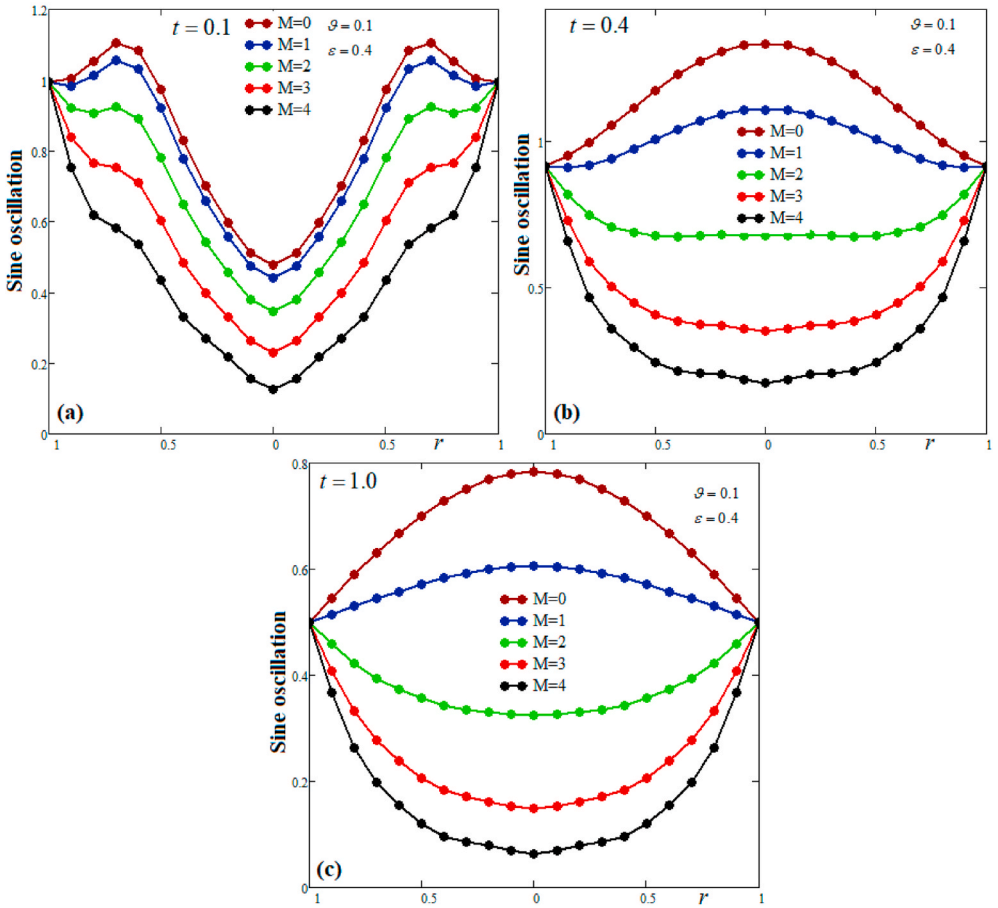

Fig. 7. (i). Profile of velocity profile with sine oscillation versus r for *M* variation at different vales of time t. Fig. 7(ii). Profile of velocity profile with cosine oscillation versus r for *M* variation at different vales of time t.

$$\Omega(\xi,t)=H(t)e^{i\omega t}-2\sum_{n=1}^{\infty}\frac{J_0(\xi\xi_n)}{\xi_n J_1(\xi_n)}\left[\delta(t)-\xi_n^2 e^{-\left(\xi_n^2+M\right)t}\right]*H(t)e^{i\omega t}+$$
$$+2Gr\sum_{n=1}^{\infty}\frac{\xi_n J_0(\xi\xi_n)}{J_1(\xi_n)}\sum_{k=0}^{\infty}\frac{(-1)^k\xi_n^{2k}}{\Pr^{k+1}(1-\vartheta)^{k+1}}G_{1,-1,\,k+1}(t,-Q)*G_{\varepsilon,\varepsilon(k+1),\,k+1}\left(t,-\frac{\vartheta}{1-\vartheta}\right)*e^{-\left(\xi_n^2+M\right)t}. \tag{58}$$

For classical case $\vartheta=1$ and $\varepsilon=0$, we get ordinary model of velocity filed as

$$\Omega(\xi,t)=H(t)e^{i\omega t}-2\sum_{n=1}^{\infty}\frac{J_0(\xi\xi_n)}{\xi_n J_1(\xi_n)}\left[\delta(t)-\xi_n^2 e^{-\left(\xi_n^2+M\right)t}\right]*H(t)e^{i\omega t}+$$
$$+2\frac{Gr}{\Pr}\sum_{n=1}^{\infty}\frac{\xi_n J_0(\xi\xi_n)}{J_1(\xi_n)}H(t)*e^{-\left(Q+\xi_n^2/\Pr\right)t}*e^{-\left(\xi_n^2+M\right)t}. \tag{59}$$

For the case, when there is no magnetic effect, consider $M=0$ in Eqs. (58) and (59), we obtain

$$\Omega(\xi,t)=H(t)e^{i\omega t}-2\sum_{n=1}^{\infty}\frac{J_0(\xi\xi_n)}{\xi_n J_1(\xi_n)}\left[\delta(t)-\xi_n^2 e^{-\xi_n^2 t}\right]*H(t)e^{i\omega t}+$$
$$+2Gr\sum_{n=1}^{\infty}\frac{\xi_n J_0(\xi\xi_n)}{J_1(\xi_n)}\sum_{k=0}^{\infty}\frac{(-1)^k\xi_n^{2k}}{\Pr^{k+1}(1-\vartheta)^{k+1}}G_{1,-1,\,k+1}(t,-Q)*G_{\varepsilon,\varepsilon(k+1),\,k+1}\left(t,-\frac{\vartheta}{1-\vartheta}\right)*e^{-\xi_n^2 t}. \tag{60}$$

For classical case $\vartheta=1$ and $\varepsilon=0$, we get ordinary model of velocity filed as

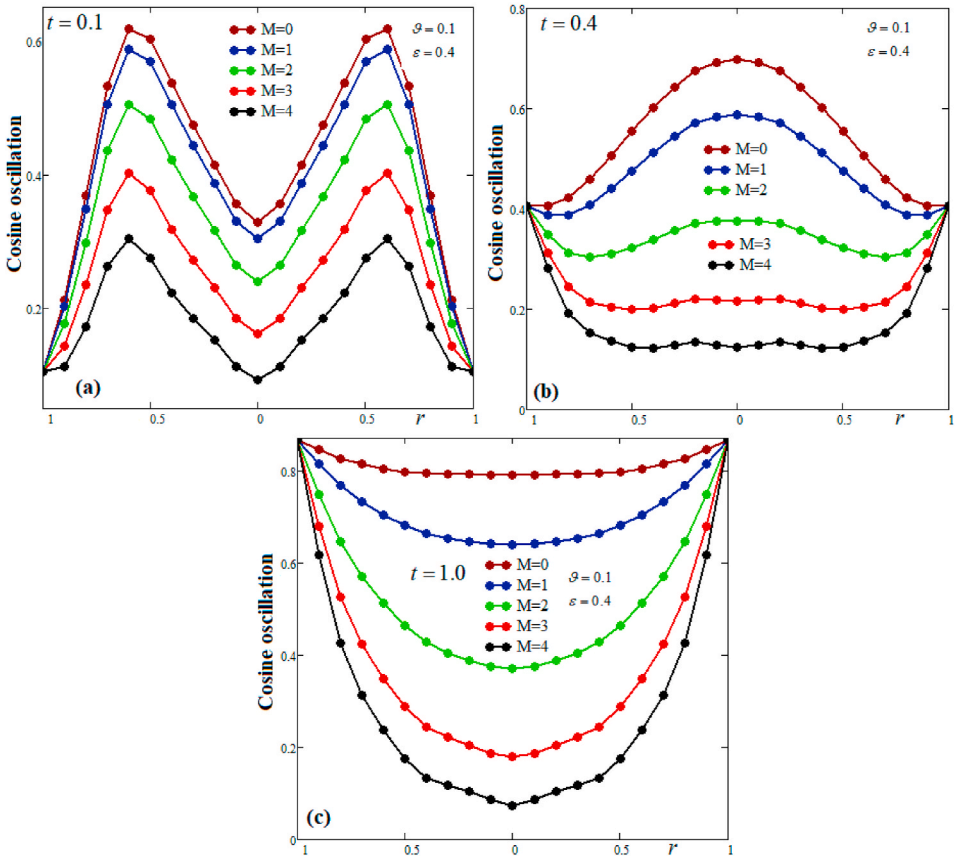

Fig. 7. (*continued*).

$$\Omega(\xi,t)=H(t)e^{i\omega t}-2\sum_{n=1}^{\infty}\frac{J_0(\xi\xi_n)}{\xi_n J_1(\xi_n)}\left[\delta(t)-\xi_n^2 e^{-\xi_n^2 t}\right]*H(t)e^{i\omega t}+$$
$$+2\frac{Gr}{\Pr}\sum_{n=1}^{\infty}\frac{\xi_n J_0(\xi\xi_n)}{J_1(\xi_n)}H(t)*e^{-\left(Q+\xi_n^2/\Pr\right)t}*e^{-\xi_n^2 t}. \tag{61}$$

4. Numerical results and discussions

In this section, we presented the numerical simulation of unsteady free convection flows of an incompressible viscous fluid with heat/sink in a vertical cylinder containing a mixture of 47 nm alumina nanoparticles in water with effect magnetic field. The generalization entails taking into account a new version of the constitutive equation for thermal flux, known as the generalized Atangana-Baleanu derivative, which is based on the generalized time-fractional derivatives with Mittag-Leffler kernel. The generalized solutions are appropriate for particularizations to yield solutions corresponding to fractional derivatives with power-law kernel and exponential kernel. The Mittag-Leffler function is a one-parametric function. It is also possible to acquire the usual situation, which corresponds to classical Fourier's law. To compare models based on generalized Atangana-Baleanu, Atangana-Baleanu, Caputo, and Caputo-Fabrizio time fractional derivatives, numerical simulations produced with the program Mathcad are carried out and visually depicted. The defaults values for fractional and physical parameters are $\vartheta = 0.1$, $\varepsilon = 0.4$, $Gr = 2$, $M = 0.2$ $Q = 0.3$, $\varphi = 0.01$, $\Pr = 4.76$.

The effects of fractional parameters ϑ and ε on temperature distribution and velocity profiles are presented in Figs. 2, 3 and 5(i), 5 (ii), 6(i) and 6(ii) for different values of time t. The important point in these graphs is that we sketch the graphs for no derivative, Caputo fractional derivative, Caputo-Fabrizio fractional derivative and Atangana-Baleanu fractional derivative as a special case of the generalized Atangana-Baleanu fractional derivative. It is observed from Fig. 2(a) for small values of time t = 0.1 temperature increased by increasing the values of fractional parameter ϑ while for t = 0.4 in Fig. 2(b) near the boundary the temperature decreased by increasing the values of ϑ but the influence is opposite in the middle of the cylinder. For t = 1 the temperature decreased by increasing the value of ϑ see Fig. 2(c). The effect of fractional parameter ϑ on velocity profile for sine and cosine oscillations are presented in Fig. 5 (i) and (ii). For small value of time t = 0.1 for sine oscillation in Fig. 5(i)(a) it is noted that near the boundary of the cylinder the velocity is decreased by increasing the values of fractional parameter ϑ while the influence is different in the middle of the cylinder. From Fig. 5

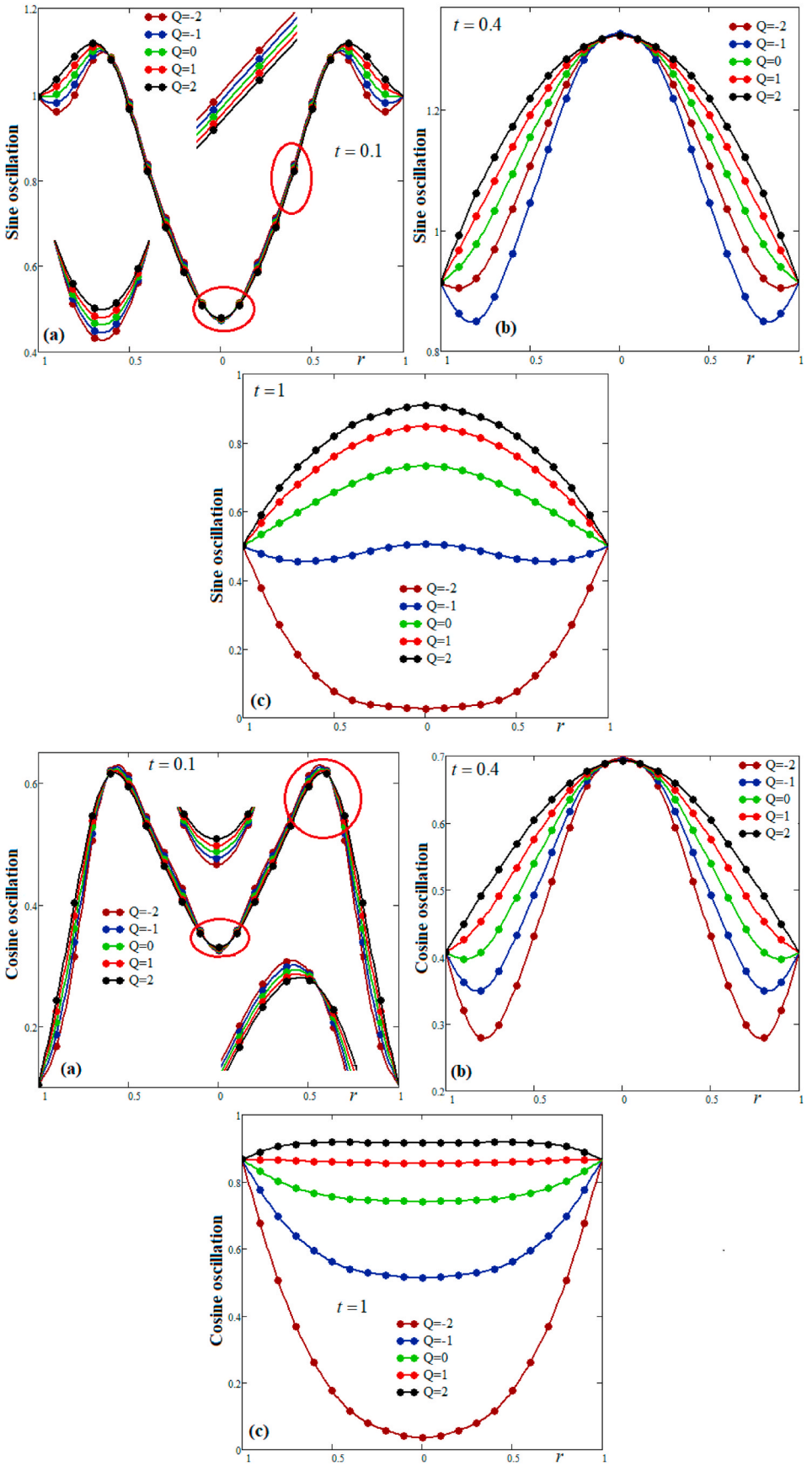

(caption on next page)

Fig. 8. (i). Profile of velocity profile with sine oscillation versus r for Q variation at different vales of time t. Fig. 8(ii). Profile of velocity profile with cosine oscillation versus r for Q variation at different vales of time t.

(i)(b) and 5(i)(c) we found that the velocity is decreased my increasing the values of fractional parameter ϑ. The same influence for the cosine oscillation in Fig. 5(ii). An interesting influence of fractional parameter ε on temperature distribution is presented in Fig. 3. For t $= 0.1$ the temperature decreases by increasing the values of ε. The temperature increased by increasing the values of ε. The effect of fractional parameter ε on velocity profile for sine and cosine oscillation is presented in Fig. 6(i) and (ii). The following observation are deduced that for $t = 0.1$ the velocity near the cylinder decreased for sine and cosine oscillations while the influence is opposite far from the boundary of the cylinder. For $t = 1$ the velocity is increased by increasing the values of fractional parameter ε. The critical values for these phase changing are around $t = 0.4$, see Fig. 6(i, ii)(b).

The effects of volume fraction φ and heat source/sink Q on temperature distribution is presented in Fig. 4. It is observed that temperature increased by increasing the values of φ. Also, the temperature layer difference decreased by increasing the values of Q. The effect of magnetic parameter M on velocity profiles are presented in Fig. 7(i) and (ii) which shows that velocity decreases by increasing the value of M as expected. In Fig. 8(i) and (ii) the effect of heat source/sink is presented. Which has an interesting influence on velocity profiles.

5. Conclusions

The concluding observations are:

F0D8 For small values of time the temperature increased by increasing the values of fractional parameters while the influence is changed by increasing the time.
F0D8 For small value of time with sine/cosine oscillations near the boundary of the cylinder the velocity is decreased by increasing the values of fractional parameters while the influence is different in the middle of the cylinder. we found that the velocity is decreased my increasing the values of fractional parameters.
F0D8 The temperature increased by increasing the values of φ.
F0D8 The temperature layer difference decreased by increasing the values of Q.
F0D8 The velocity decreases by increasing the value of M.

Author statement

NAS: Conceptualization; AW: Data curation; RS AND YM: Formal analysis; NAS, AW AND KH Writing - original draft; Methodology; BS AND SJY: Investigation; NAS AND RS: Resources; Writing - review & editing; SJY: Supervision.

Declaration of competing interest

The authors declare that they have no known competing financial interests or personal relationships that could have appeared to influence the work reported in this paper.

Acknowledgments

This work was conducted under the Technology Innovation Program (or Industrial Strategic Technology Development Program material part package type) as “Development of fire suppression-type high safety module and demonstration of safety for future ecofriendly medium and large secondary battery (No. 20015986)”, funded by the Ministry of Trade, Industry & Energy (MOTIE), Republic of Korea and Researchers Supporting Project number (RSP-2021/145), King Saud University, Riyadh, Saudi Arabia.

References

[1] L. Debnath, On unsteady magnetohydrodynamic boundary layers in a rotating flow, ZAMM - Zeitschrift Fur Angewandte Mathematik Und Mechanik 52 (10) (1972) 623–626.
[2] L. Deng, T. Li, M. Bi, J. Liu, M. Peng, Dependence of tropical cyclone development on coriolis parameter: a theoretical model, Dynam. Atmos. Oceans 81 (2018) 51–62.
[3] Z. Du, M.S. Selig, The effect of rotation on the boundary layer of a wind turbine blade, Renew. Energy 20 (2) (2000) 167–181.
[4] A. Paul, R.K. Deka, Unsteady natural convection flow past an infinite cylinder with thermal and mass stratification, Int. J. Eng. Math. (2017) 13. Article ID 8410691.
[5] N.B. Totala, M.V. Shimpi, N.L. Shete, V.S. Bhopate, Natural convection characteristics in vertical cylinder, Int. J. Eng. Sci. 3 (8) (2013) 27–31.
[6] F. Moukalled, S. Acharya, Natural convection in the annulus between concentric circular and square cylinders, J. Thermophys. Heat Tran. 10 (3) (1996) 524–531.
[7] S.U. Choi, J.A. Eastman, Enhancing Thermal Conductivity of Fluids with Nanoparticles (No. ANL/MSD/CP-84938, CONF-951135-29), Argonne National Lab., IL (United States), 1995.
[8] K.V. Wong, O. De Leon, Applications of nanouids: current and future, Adv. Mech. Eng. 2 (2010) 519659.
[9] C.T. Nguyen, F. Desgranges, G. Roy, N. Galanis, T. Mare, S. Boucher, H. Angue Mintsa, Temperature and particle-size dependent viscosity data for water-based nanofluids Hysteresis phenomenon, Int. J. Heat Fluid Flow 28 (6) (2007) 1492–1506.

[10] M. Ali, A.A. Shoukat, H.A. Tariq, M. Anwar, H. Ali, Header design optimization of mini-channel heat sinks using CuO-H_2O and Al_2O_3-H_2O nanofluids for thermal management, Arabian J. Sci. Eng. 44 (2019) 10327–10338.
[11] M. Caputo, F. Mainardi, Linear models of dissipation in anelastic solids, Riv. Nuovo Cimento 1 (1971) 161–198.
[12] R.J. Marks II, M.W. Hall, Differ-integral interpolation from a bandlimited signal's samples, IEEE Trans. Acoust. Speech Signal Process. 29 (1981) 872–877.
[13] W.E. Olmstead, R.A. Handelsman, Diffusion in a semi-infinite region with nonlinear surface dissipation, SIAM Rev. 18 (1976) 275–291.
[14] K. Diethelm, A.D. Freed, On the solution of nonlinear fractional differential equations used in the modeling of viscoelasticity, in: F. Keil, W. Mackens, H. Voß, J. Werther (Eds.), Scientific Computing in Chemical Engineering II: Computational Fluid Dynamics, Reaction Engineering, and Molecular Properties, Springer, Heidelberg, 1999, pp. 217–224.
[15] L. Gaul, P. Klein, S. Kempfle, Damping description involving fractional operators, Mech. Syst. Signal Process. 5 (1991) 81–88.
[16] W.G. Glöckle, T.F. Nonnenmacher, A fractional calculus approach to self-similar protein dynamics, Biophys. J. 68 (1995) 46–53.
[17] J. Hristov, Bio-heat models revisited: concepts, derivations, nondimensalization and fractionalization attempts, Front. Physiol. 7 (2019) 189, https://doi.org/10.3389/fphy.2019.001897.
[18] A. Fabre, J. Hristov, Transient Heat conduction in materials with linear power-law temperature-dependent thermal conductivity: integral-Balance Approach, Fluid Dynam. Mater. Process. 12 (2) (2016) 69–85.
[19] K. Diethelm, N.J. Ford, A.D. Freed, Yu. Luchko, Algorithms for the fractional calculus: a selection of numerical methods, Comput. Methods Appl. Mech. Eng. 194 (2005) 743–773.
[20] O.D. Makinde, I.L. Animasaun, Bioconvection in MHD nanofluid flow with nonlinear thermal radiation and quartic autocatalysis chemical reaction past an upper surface of a paraboloid of revolution, Int. J. Therm. Sci. 109 (2016) 159–171.
[21] M. Sheikholeslami, H.R. Kataria, A.S. Mittal, Effect of thermal diffusion and heat-generation on MHD nanofluid flow past an oscillating vertical plate through porous medium, J. Mol. Liq. 257 (2018) 12–25.
[22] M. Azam, A. Shakoor, H.F. Rasool, M. Khan, Numerical simulation for solar energy aspects on unsteady convective flow of MHD Cross nanofluid: a revised approach, Int. J. Heat Mass Tran. 131 (2019) 495–505.
[23] Z. Shao, N.A. Shah, I. Tlili, U. Afzal, M.S. Khan, Hydromagnetic free convection flow of viscous fluid between vertical parallel plates with damped thermal and mass fluxes, Alexandria Eng. J. 58 (2019) 989–1000.
[24] C. Fetecau, N.A. Shah, D. Vieru, General solutions for hydromagnetic free convection flow over an infinite plate with Newtonian heating, mass diffusion and chemical reaction, Commun. Theor. Phys. 68 (2017) 768–782.
[25] D. Yadav, D. Nam, J. Lee, The onset of transient Soret-driven MHD convection confined within a Hele-Shaw cell with nanoparticles suspension, J. Taiwan Inst. Chem E. 58 (2016) 235–244.
[26] A.U. Awan, N.A. Shah, N. Ahmed, Q. Ali, S. Riaz, Analysis of free convection flow of viscous fluid with damped thermal and mass fluxes, Chin. J. Phys. 60 (2019) 98–106.
[27] Y. Tan, Y. Zheng, N. Wang, et al., Controlling the properties of solvent-free FO3O4 nanofluids by corona structure, Nano-Micro Lett. 4 (2012) 208–214.
[28] N.A. Shah, A. Hajizadeh, M. Zeb, S. Ahmad, Y. Mahsud, I.L. Animasaun, Effect of magnetic field on double convection flow of viscous fluid over a moving vertical plate with constant temperature and general concentration by using new trend of fractional derivative, Open J. Math. Sci. 2 (1) (2018) 253–265.
[29] Xiao, Y. Shah, N. A., Irshad, T., Magneto-hydrodynamics natural convection flows of viscous carbon nanotubes nanofluids with generalized Fourier's law in a vertical cylinder, https://doi.org/10.1002/mma.6566.
[30] R. Gorenflo, A.A. Kilbas, F. Mainardi, S.V. Rogosin, Mittag-Leffler Functions, Related Topics and Applications, Springer Monographs in Mathematics, 2014, https://doi.org/10.1007/978-3-662-43930-2.
[31] E.C. Grigoletto, E.C. Oliveira, R.F. Camargo, Integral representations of Mittag-Leffler function on the positive real axis, Tendencias em Matematica Aplicada e Computacional 20 (2) (2019) 217–228, https://doi.org/10.5540/tema.2019.020.02.0217.
[32] K. Diethelm, N.J. Ford, A.D. Freed, Yu. Luchko, Algorithms for the fractional calculus: a selection of numerical methods, Comput. Methods Appl. Mech. Eng. 194 (2005) 743–773.
[33] D. Vieru, C. Fetecau, N. Ahmed, N.A. Shah, A generalized kinetic model of the advection-dispersion process in a sorbing medium, Math. Model Nat. Phenom. 16 (2021) 39.
[34] A.S. Oke, I.L. Animasaun, W.N. Mutuku, M. Kimathi, N.A. Shah, S. Saleem, Significance of Coriolis force, volume fraction, and heat source/sink on the dynamics of water conveying 47 nm alumina nanoparticles over a uniform surface, Chin. J. Phys. 71 (2021) 716–727.
[35] Y. Xuan, W. Roetzel, Conceptions for heat transfer correlation of nanofluids, Int. J. Heat Mass Tran. 43 (19) (2000) 3701–3707.